

# Integration of cell differentiation and initiation of monoterpenoid indole alkaloid metabolism in seed germination of *Catharanthus roseus*

Mai Uzaki<sup>1,2</sup> , Tetsuya Mori<sup>2</sup> , Mayuko Sato<sup>2</sup>, Mayumi Wakazaki<sup>2</sup>, Noriko Takeda-Kamiya<sup>2</sup>, Kotaro Yamamoto<sup>3</sup> , Akio Murakami<sup>4</sup> , Delia Ayled Serna Guerrero<sup>5</sup> , Chizuko Shichijo<sup>4</sup>, Miwa Ohnishi<sup>4,6</sup>, Kimitsune Ishizaki<sup>4</sup> , Hidehiro Fukaki<sup>4</sup> , Sarah E. O'Connor<sup>5</sup> , Kiminori Toyooka<sup>2</sup> , Tetsuro Mimura<sup>4,7,8,9</sup>  and Masami Yokota Hirai<sup>1,2</sup> 

<sup>1</sup>Graduate School of Bioagricultural Science, Nagoya University, Nagoya, Aichi, 464-8601, Japan; <sup>2</sup>RIKEN Center for Sustainable Resource Science, Yokohama, Kanagawa, 230-0045, Japan;

<sup>3</sup>School of Science, Yokohama City University, Yokohama, Kanagawa, 236-0027, Japan; <sup>4</sup>Graduate School of Science, Kobe University, Kobe, Hyogo, 657-8501, Japan; <sup>5</sup>Department of

Natural Product Biosynthesis, Max Planck Institute for Chemical Ecology, Jena, D-07745, Germany; <sup>6</sup>Graduate School of Science, Kyoto University, Kyoto, 606-8502, Japan; <sup>7</sup>College of

Bioscience and Biotechnology, National Cheng Kung University, Tainan, 70101, Taiwan; <sup>8</sup>The Institute for Sustainable Agro-ecosystem Services, Graduate School of Agricultural and

Life Sciences, The University of Tokyo, Tokyo, 188-0002, Japan; <sup>9</sup>Faculty of Bioenvironmental Sciences, Kyoto University of Advanced Science, Kyoto, 621-8555, Japan

## Summary

Authors for correspondence:

Masami Yokota Hirai

Email: [masami.hirai@riken.jp](mailto:masami.hirai@riken.jp)

Tetsuro Mimura

Email: [mimura.tetsuro@kuas.ac.jp](mailto:mimura.tetsuro@kuas.ac.jp)

Received: 1 December 2023

Accepted: 22 February 2024

New Phytologist (2024)

doi: 10.1111/nph.19662

**Key words:** *Catharanthus roseus*, cell differentiation, idioblast, laticifer, metabolic differentiation, monoterpenoid indole alkaloid, seed germination.

- In *Catharanthus roseus*, monoterpenoid indole alkaloids (MIAs) are produced through the cooperation of four cell types, with final products accumulating in specialized cells known as idioblasts and laticifers. To explore the relationship between cellular differentiation and cell type-specific MIA metabolism, we analyzed the expression of MIA biosynthesis in germinating seeds.
- Embryos from immature and mature seeds were observed via stereomicroscopy, fluorescence microscopy, and electron microscopy. Time-series MIA and iridoid quantification, along with transcriptome analysis, were conducted to determine the initiation of MIA biosynthesis. In addition, the localization of MIAs was examined using alkaloid staining and imaging mass spectrometry (IMS).
- Laticifers were present in embryos before seed maturation. MIA biosynthesis commenced 12 h after germination. MIAs accumulated in laticifers of embryos following seed germination, and MIA metabolism is induced after germination in a tissue-specific manner.
- These findings suggest that cellular morphological differentiation precedes metabolic differentiation. Considering the well-known toxicity and defense role of MIAs in matured plants, MIAs may be an important defense strategy already in the delicate developmental phase of seed germination, and biosynthesis and accumulation of MIAs may require the tissue and cellular differentiation.

## Introduction

Plants, bacteria, and fungi produce various species-specific compounds known as specialized metabolites (formerly referred to as secondary metabolites). These metabolites, although not essential for the survival of these organisms, are crucial for their environmental adaptation and interactions with other organisms. They are of significant interest due to their roles in everyday human life, including in drugs, fragrances, and dyes. Consequently, specialized metabolism has been extensively studied, including the chemical structure and physiological properties of metabolites themselves, but also at the protein/gene level of enzymes of the biosynthetic pathways, transporters, and transcription factors (TFs; Weng *et al.*, 2021). In plants, many of these metabolites

are biosynthesized and stored in specific cells. For instance, artemisinin from *Artemisia annua*, which is used as an antimalarial drug, is produced and specifically accumulated in glandular trichomes (Olsson *et al.*, 2009). Morphine in *Papaver somniferum* is biosynthesized in sieve elements and laticifers (Onoyovwe *et al.*, 2013), while glucosinolates in *Arabidopsis thaliana* are generated in S-cells and surrounding sieve elements, accumulating specifically in S cells (Koroleva *et al.*, 2000). This compartmentalization is thought to be a strategy to isolate bioactive, potentially self-toxic compounds from other cells within the plant (Foster, 1955), but the precise physiological importance of this mechanism remains unclear.

*Catharanthus roseus* (Apocynaceae) is a well-known medicinal plant that produces > 130 types of monoterpenoid indole alkaloid

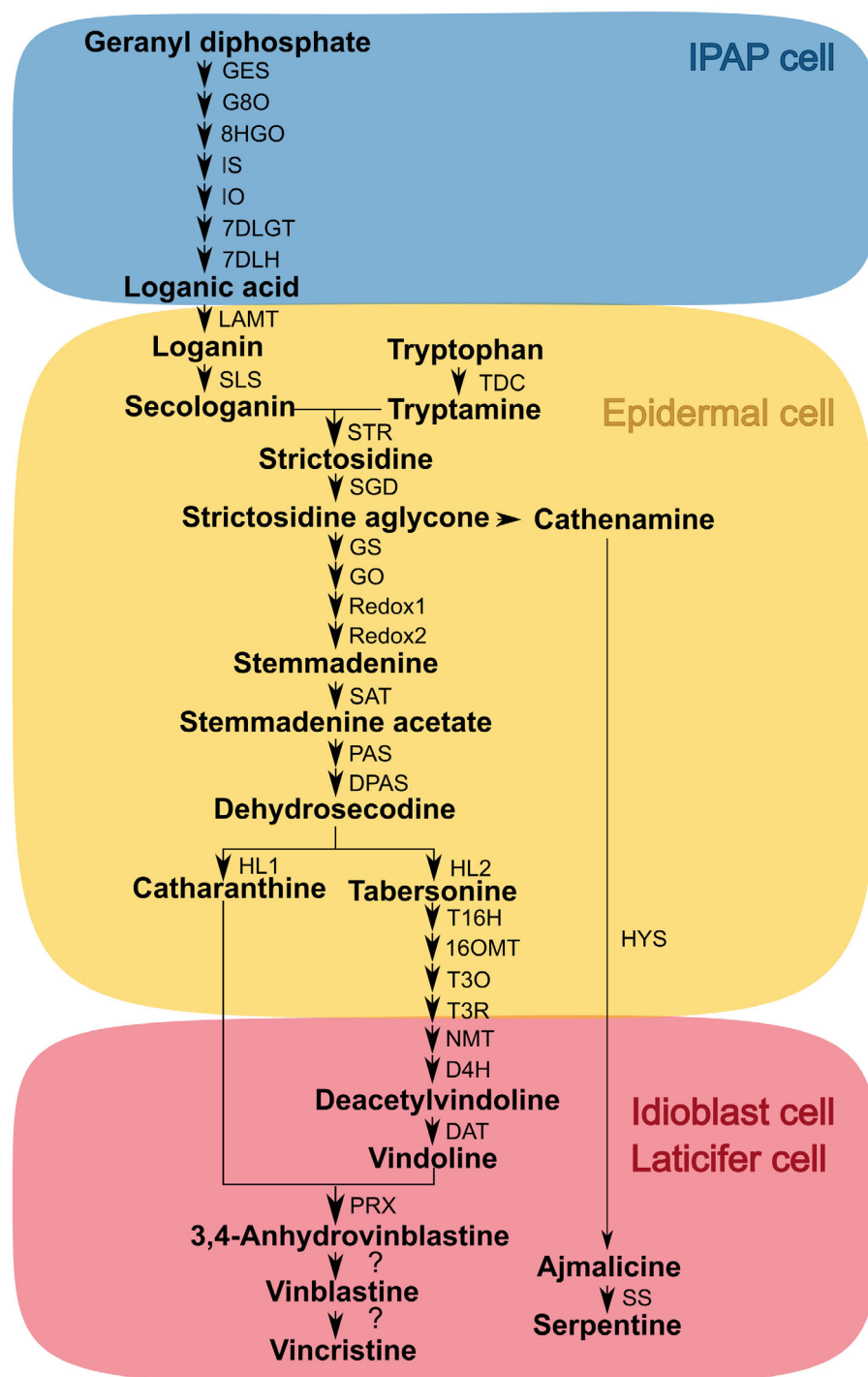


**Fig. 1** Schematic of the monoterpene indole alkaloid (MIA) biosynthetic pathway of *Catharanthus roseus*. 16OMT, tabersonine 16-O-methyltransferase; 7DLGT, 7-deoxyloganic acid glucosyl transferase; 7DLH, 7-deoxyloganic acid hydroxylase; 8HGO, 8-hydroxygeraniol oxidoreductase; D4H, deacetoxyvindoline 4-hydroxylase; DAT, deacetylvindoline O-acetyltransferase; DPAS, dihydroprecondylocarpine acetate synthase; G8O, geraniol 8-oxidase; GES, geraniol synthase; GO, geissoschizine oxidase; GS, geissoschizine synthase; HL1, hydrolase1; HL2, hydrolase2; HYS, heteroyohimbine synthase; IO, iridoid oxidase; IPAP cell, internal phloem-associated parenchyma cell; IS, iridoid synthase; LAMT, loganic acid methyl transferase; NMT, 3-hydroxy-16-methoxy-2,3-dihydrotabersonine N-methyltransferase; PAS, precondylocarpine acetate synthase; PRX, peroxidase; SAT, stemmadenine O-acetyltransferase; SGD, strictosidine beta-glucosidase; SLS, secologanin synthase; SS, serpentine synthase; STR, strictosidine synthase; T16H, tabersonine 16-hydroxylase; T3O, tabersonine 3-oxygenase; T3R, 16-methoxy-2,3-dihydro-3-hydroxytabersonine synthase; TDC, tryptamine decarboxylase.

(MIA; Van Der Heijden *et al.*, 2004). These MIAs are thought to be important for defense against pests and in the stress response: The MIA biosynthetic pathway is partially activated by the stress hormone jasmonate (Dugé De Bernonville *et al.*, 2017). The biosynthetic pathways of MIAs, including medically important ones such as vinblastine and vincristine, have been well studied (Kulagina *et al.*, 2022). MIAs are biosynthesized through the collaboration of four cell types, namely internal phloem-associated parenchyma (IPAP) cells, epidermal cells, idioblasts, and laticifers

(Fig. 1), with the final products, and intermediate accumulating in the latter two (St-Pierre *et al.*, 1999; Miettinen *et al.*, 2014; Yamamoto *et al.*, 2016, 2019; Sun *et al.*, 2022; Li *et al.*, 2023; Guedes *et al.*, 2024).

Idioblasts are distinguished by their unique morphology compared with surrounding cells (Foster, 1955). Their characteristics vary widely and include a variety of cells such as S-cells and myrosin cells in *A. thaliana* (Koroleva *et al.*, 2000; Shirakawa *et al.*, 2014), fluorescent idioblasts in *Egeria densa* (Hara *et al.*,

2015), and oilbody cells in *Marcantia polymorpha* (Suire, 2000; Kanazawa *et al.*, 2020). Tubular idioblasts that accumulate latex are termed laticifers (Esau, 1965). These cells are found across diverse plant groups, from mosses to angiosperms, and are often associated with specialized metabolism (Hagel *et al.*, 2008). *C. roseus* has globular and tubular idioblasts; the former is often referred to as idioblasts and the latter as laticifers. These cells are found in every tissue in *C. roseus* plant.

The morphological differentiation of laticifers has been studied in various plants. Laticifers are categorized into four types: articulated-anastomosing, articulated-nonanastomosing, nonarticulated-branched, and nonarticulated-unbranched (Esau, 1965). *C. roseus* laticifers fall into the nonarticulated-unbranched category. Nonarticulated laticifers originate from a single cell, forming a tubular structure; they are multinucleated due to cell division without cell plate formation (Esau, 1965; Wilson & Mahlberg, 1978). While nonarticulated-branched laticifers have been extensively studied, less is known about nonarticulated-unbranched laticifers (Mahlberg, 1961; Castelblanque *et al.*, 2016).

A study on *Papaver bracteatum* established a link between increases in alkaloid level and the development of articulated laticifers in germinating seed embryos (Rush *et al.*, 1985). Castelblanque *et al.* (2016) demonstrated that mutants with impaired laticifer formation produced less triterpene, suggesting a connection between laticifer differentiation and specialized metabolism. Similarly, *C. roseus* cells showed reduced MIA production during dedifferentiation, indicating a close relationship between MIA biosynthesis and cellular differentiation (Datta & Srivastava, 1997). However, the specifics of the onset of specialized metabolism and the metabolic differentiation of various cell types during plant development are not fully understood.

In this study, we investigated the relationship between the initiation of cell type-specific MIA metabolism and cellular differentiating state, focusing on embryos of germinating seeds. We found that laticifers in developing embryos were morphologically differentiated and noted gradual induction of MIA biosynthesis during germination, with variation in the timing of MIA biosynthetic gene expression. MIA metabolism primarily occurred in roots and hypocotyls 24–48 h after germination (HAG) and was not observed in cotyledons, suggesting later metabolic differentiation in cotyledons. These findings highlight the importance of organ development stages and cell differentiation in the initiation of MIA metabolism during embryogenesis and germination in *C. roseus*.

## Materials and Methods

### Plant materials and culture

*Catharanthus roseus* (L.) G. Don (cv Equator White Eye) seeds were obtained from Sakata Seed Corp. (Kanagawa, Japan). The mature seeds were sterilized by soaking in 70% ethanol for 10 min and then treated with 3% sodium hypochlorite containing 0.2% Triton X-100 for 10 min with vortexing. Subsequently, the seeds were washed with sterile water for 10 min. Sterilized

seeds were incubated on 0.8% agar plates (ultrapure water solidified with agar, without any nutrients) at 25°C in darkness in an incubator (BR-43FL; Taitec, Saitama, Japan). For light condition experiments, 0 HAG seed plates were transferred to a growth chamber with white fluorescent light (Nippon Medical & Chemical Instruments Co., Ltd, Osaka, Japan), under a 16 h : 8 h, light : dark photoperiod.

For MIA extraction from leaves, stems, hypocotyls, and roots, 2-month-old plants with three leaf pairs were used. These plants were cultivated in a mixture of PRO-MIX BX (Premier Horticulture, Rivière-du-Loup, QC, Canada) and vermiculite (VS Kakou Corp., Tokyo, Japan) in a prefabricated room-type chamber at 22°C under a 16 h photoperiod. The plants were watered twice weekly with MGRL medium (Fujiwara *et al.*, 1992). Collected samples were observed either via microscopy or immediately frozen in liquid nitrogen and stored at –80°C until further use.

### Microscopic observation

Whole embryos dissected from immature or mature seeds were examined under a stereomicroscope (MZ10FA; Leica Microsystems, Wetzlar, Germany) and a fluorescence microscope (BX53; Olympus, Tokyo, Japan). The fluorescence microscope was equipped with a 100 W mercury lamp and a U-FUW mirror unit providing an excitation wavelength range of 340–390 nm and an emission wavelength of 420 nm and longer.

### Compound extraction

Compound extraction involved using 10 embryos (*c.* 1–3 mg dry weight) or endosperms with seed coat (*c.* 10 mg dry weight), or 3.0 mg dry weight mature leaves, stems, hypocotyls, and roots per sample. Samples were lyophilized in a dry chamber (DRC-1000; Eyela, Tokyo, Japan) equipped with a freeze dryer (FDU-2100; Eyela) and pulverized into a fine powder using a bead crusher (Shake Master NEO; BioMedical Science, Tokyo, Japan). Then, 0.5 ml methanol containing 20 ng ml<sup>-1</sup> ajmaline was added to the powdered samples and mixed by inversion for 1 h. The supernatant was collected, and the procedure was repeated with another 0.5 ml methanol containing 20 ng ml<sup>-1</sup> ajmaline added to the residue. The two supernatants were combined and filtered through a 0.2 µm diameter filter (Millex-LG Syringe Driven Filter Unit SLLGH04NL; Merck, Millipore, MA, USA) for measurement.

### Analysis of MIAs and iridoids by liquid chromatography–tandem mass spectrometry

The analysis of MIAs and iridoids, extracted as described above, was conducted using an ultrahigh-performance liquid chromatography (UPLC) system (Nexera X2; Shimadzu Co., Kyoto, Japan). This was followed by electrospray injection into a triple quadrupole tandem mass spectrometer (LCMS-8050; Shimadzu Co.).

For MIA chromatographic separation, a C18 column (Kinetex 2.6 µm XB-C18 100 Å, LC column 100 × 2.1 mm; Phenomenex Co., Torrance, CA, USA) was used, employing a method outlined

in prior research (Stavrinides *et al.*, 2015). The mobile phase consisted of (A) 0.1% (v/v) formic acid and (B) acetonitrile. The elution program was as follows: 10–30% B (0–5.0 min), 30–100% B (5.0–6.0 min), 100% B (6.0–7.5 min), 100–10% (7.5–8.0 min) and 10% B (8.0–10.0 min). The column temperature was maintained at 40°C, with a flow rate of 0.6 ml min<sup>-1</sup> and an injection volume of 1.0 µl.

For iridoid separation, an ACQUITY UPLC BEH C18 Column (130 Å, 1.7 µm, 2.1 mm × 50 mm; Waters Co., Milford, MA, USA) was used. The mobile phase consisted of (A) 0.1% (v/v) formic acid and (B) acetonitrile. The elution program for iridoids was optimized as follows: 8% B (0–0.5 min), 8–20% B (0.5–3.0 min), 20% B (3.0–3.3 min), 20–100% B (3.3–4.0 min), 100% B (4.0–5.0 min), and 8% B (5.5–7.0 min). The column temperature was kept at 40°C with a flow rate of 0.3 ml min<sup>-1</sup> and an injection volume of 1.0 µl.

Mass spectrometry (MS) detection was performed using an electrospray ionization source in positive-ion detection mode and operated in multiple reaction monitoring (MRM) mode. The MRM transitions used to monitor the elution are listed in Supporting Information Table S1. More than five biological replicates were performed for each analysis.

The standard compound was measured multiple times via LC–MS/MS, and the most diluted concentration yielding a relative standard deviation < 10% was set as the limit of quantification.

Data analysis was carried out using LABSOLUTIONS LCMS v.5.97 SP1 (Shimadzu Co.). The processed data were visualized using R 3.6.3 (R Core Team, 2020). Data shaping employed the TIDYVERSE (Wickham *et al.*, 2019), DPLYR (Wickham *et al.*, 2023), STRINGR (Wickham, 2023), and HMISC (Harrell Jr & Dupont, 2019) packages. Bar graphs of MIA/iridoid concentration were generated using GGPLOT2 (Wickham, 2016) and GGPRISM (Dawson, 2022) packages.

Commercially available standard chemicals, tryptamine (Sigma-Aldrich Co. LLC), catharanthine (Enzo Life Sciences, New York, NY, USA), tabersonine HCl (AvaChem Scientific, San Antonio, TX, USA), ajmalicine (AdipoGen Life Sciences, Liestal, Switzerland), serpentine hydrogen tartrate (ChromaDex, Irvine, CA, USA), deacetylvindoline (Toronto Research Chemicals, North York, ON, Canada), vindoline (ChromaDex), 3,4-anhydrovinblastine sulfate (Toronto Research Chemicals), vinblastine sulfate (Toronto Research Chemicals), and vincristine sulfate (Toronto Research Chemicals) were purchased, and strictonine was produced in Dr Sarah E. O'Connor's laboratory. These commercial chemicals were used as standards for MIA quantification. Ajmaline was purchased from Toronto Research Chemicals and used as an internal standard.

### Imaging mass spectrometry analysis

The preparation of frozen sections for imaging mass spectrometry (IMS) analysis followed a protocol established in previous research (Nakabayashi *et al.*, 2019). Collected germinating seeds of *C. roseus* were embedded in Surgipath FSC22 compound (Leica Microsystems) and frozen in a -75°C acetone bath

(Histo-Tek Pino; Sakura Finetek Japan Co., Ltd, Tokyo, Japan). Then, the frozen block was sectioned with a knife blade until the desired tissue surface was exposed. Transfer tape (Adhesive Tape Windows; Leica Microsystems) was applied to the face of the block, and 11 µm sections were produced using a cryostat (CM3050S; Leica Microsystems). Then, the sections attached to the transfer tape were transferred to conductive copper tape (double-sided No. 796; Teraoka Seisakusho Co., Ltd, Tokyo, Japan) on an ITO-coated glass slide (Bruker Daltonics GmbH, Billerica, MA, USA). These sections were subsequently freeze-dried overnight at -30°C.

An  $\alpha$ -cyano-4-hydroxycinnamic acid (CHCA) matrix solution was sprayed onto the prepared sections on the glass slides using a TM-Sprayer (HTX Technologies, LLC, Chapel Hill, NC, USA). Then, these were analyzed via Fourier transform ion cyclotron resonance mass spectrometry (FTICR-MS; Solarix 7.0 T; Bruker Daltonics Inc.). Matrix-assisted laser desorption/ionization (MALDI)-IMS was conducted in positive-ion detection mode, covering a mass range of  $m/z$  150–600 with 30 µm spatial resolution (Fig. S1). Visualization analysis was performed using SCiLS LAB software v.2023a Core (Bruker Daltonics Inc.).

## Results

### Establishment of a time-series sampling method for germinating seeds

To examine the early developmental regulation of the MIA pathway, a method for sampling embryos of germinating seeds was established. Microscopic observation was used to define imbibition start time and germination time. The end of seed sterilization was marked as the start of imbibition (0 h after start of imbibition; 0 HAI). Embryos and endosperms were separately collected at 8, 16, 24, and 32 HAI (Fig. 2). For the 32 HAI samples, only ungerminated seeds were included, as some seeds had germinated by this time. Due to the asynchronous germination of *C. roseus* seeds (Fig. S2), the imbibing seeds were monitored every 2 h from 30 HAI. Seeds showing seed coat rupture were considered 0 HAG seeds and were transferred to a new agar plate. Subsequent sampling of embryos and endosperms occurred at 12, 24, 36, 48, and 60 HAG (Fig. 2). However, our endosperm samples contain the seed coat because it is quite difficult to remove the seed coat from small seeds of *C. roseus*.

### Idioblasts and laticifers morphologically differentiate in embryos during seed maturation

After flowering and fertilization, *C. roseus* produces siliques containing 1–20 seeds (Fig. 3a,b). Immature seeds are characterized by green, soft seed coats, which harden and darken as they mature. Once mature, the silique breaks open, revealing the black, hardened seeds.

We first observed the embryos dissected from immature (Figs 2a, 3c–f) and mature seeds (Figs 2b, 3b,i) under a stereomicroscope and a fluorescence microscope to see whether idioblasts and laticifers were morphologically differentiated at this time,

## (a) Maturation of seeds in silique



## (b) Imbibition and germination of seeds

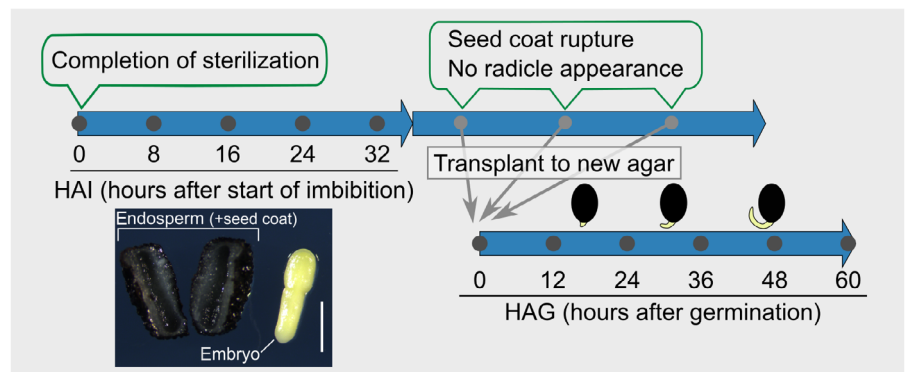


**Fig. 2** Timetable for processing and sampling of seeds of *Catharanthus roseus*. (a) Seed maturation process in *C. roseus*, highlighting the nonsynchronized maturation of seeds. Immature seeds were randomly collected, with maturity inferred from their appearance. (b) Sampling methodology for imbibing/germinating seeds. The start of imbibition is marked by the end of seed sterilization. Embryos and endosperms were collected every 8 h up to 32 h after start of imbibition (HAI). Seed coat rupture, indicative of germination commencement, was monitored every 2 h after 30 h of imbibition. Seeds were sampled at intervals of 12 h up to 60 h after germination (HAG). Bar: 1 mm.

because idioblasts and laticifers in leaves or stems typically exhibit fluorescent granular or elongated shapes (St-Pierre *et al.*, 1999; Yamamoto *et al.*, 2016, 2019; Uzaki *et al.*, 2022). Embryos from immature seeds displayed red autofluorescence from chlorophyll and blue autofluorescence from unidentified substances in the radicle (Fig. 3c,d). Fluorescent, laticifer-like elongated structures were observed in some embryos as the seed coat hardened (Fig. 3e,g,h), indicating that laticifers had morphologically differentiated and accumulated fluorescent compounds at this stage. However, in more mature seeds, these fluorescent laticifers were not evident (Fig. 3f).

Embryos from dried, mature seeds before germination showed blue autofluorescence throughout, and fluorescent laticifer-like structures were not observed (Fig. 3i 8 HAI and 0 HAG). These structures reappeared in roots at 24 HAG and in hypocotyls at 36 HAG, and a few fluorescent idioblasts were noted in embryos at 48 HAG and 60 HAG. They were also present in cotyledons at 60 HAG. Sectioning of 48 HAG embryos revealed fluorescent cells exist at the periphery (Fig. S3a,c), where laticifers are expected to be located, with xylem displaying spiral structures at the center (Fig. S3d,f). Laticifers in many plant species, including *C. roseus*, accumulate lipids (Castelblanque *et al.*, 2016). Staining of 48 HAG seed embryos with Nile blue, a marker for fatty acid and lipid-soluble compounds, also highlighted these fluorescent elongated structures as in laticifers in leaves (Methods S1, Fig. S4). These observations suggest that the fluorescent, elongated structures seen after germination of embryos were indeed laticifers.

Composition of fluorescent compound in embryos seem to be different from that of mature leaf and stem

We then investigated whether the fluorescent compounds accumulated in embryonic laticifers were the same as those in mature

plants (Methods S2). Analysis of *in situ* single laticifers via fluorescent microscopy suggested a distinct composition of fluorescent compounds compared with those in laticifers of leaves and stems (Fig. S5a). In addition, methanol extracts of whole embryos from 48 HAG seeds and extracts from leaves, stems, and roots were analyzed using a liquid chromatography (LC)-fluorescence detector (Methods S3). The extract from leaves and stems predominantly showed a peak with a retention time (RT) corresponding to serpentine. The root extract, however, revealed two additional peaks of unknown compounds in addition to the serpentine peak. The endosperm extract exhibited a peak with a slightly different RT from serpentine, suggesting that fluorescence in endosperm did not originate from serpentine. The embryo extract contained four fluorescent compounds, including a small peak with an RT-matching serpentine, and the elution pattern was similar to that of the extract from roots (Fig. S5b).

These findings suggest that laticifers in embryos of developing immature seeds undergo morphological differentiation and transiently accumulate cell type-specific fluorescent metabolites. In germinating seed embryos, certain fluorescent compounds are specifically accumulated in laticifers after 24 HAG.

#### Intracellular structures in laticifers changed dramatically during seed maturation and germination

To examine intracellular structural changes in laticifers during seed maturation and germination, resin-embedded semithin sections of embryos from immature seeds and seeds at 0 HAG, 12 HAG, 24 HAG, and 36 HAG were examined using an upright microscope and field emission scanning electron microscopy (FE-SEM) (Methods S4, S5). We focused on laticifers in the hypocotyl, as idioblasts were not morphologically distinct from other cells at these stages.

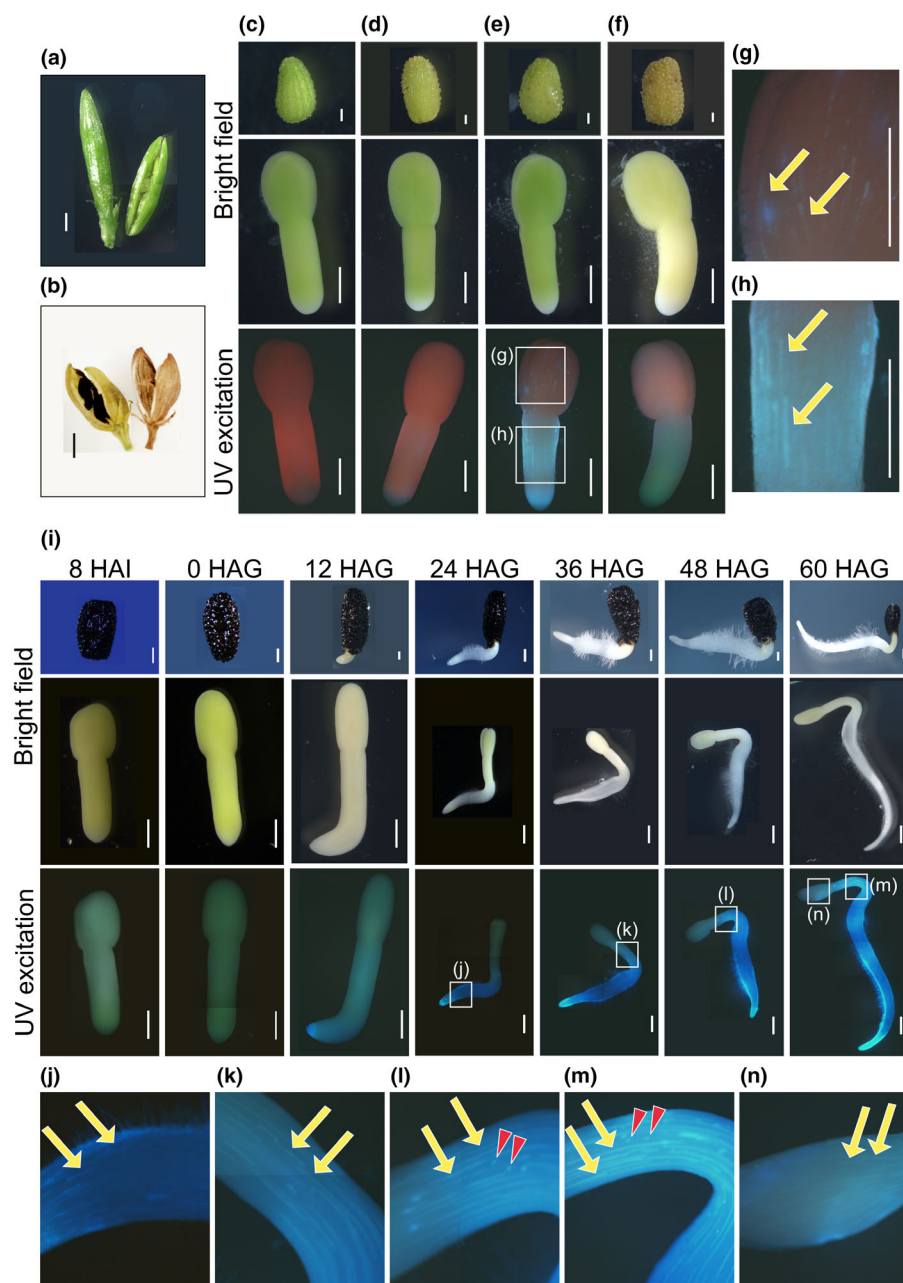


**Fig. 3** Microscopic images of seeds and embryos of *Catharanthus roseus*. (a) Immature siliques of *C. roseus*. (b) Mature siliques and seeds. (c–f) Microphotographs of immature seeds (top) and embryos (middle and bottom), with seed coats progressively hardening and drying from c to f. (g, h) Magnification of boxed areas in (e), with yellow arrows indicating laticifer-like structures. (i) Microphotographs of matured (8 h after start of imbibition, HAI) and germinating (0–60 h after germination, HAG) seeds (top) and embryos dissected from the seeds (middle and bottom). Time points (8 HAI–60 HAG) correspond to those detailed in Fig. 2. (j–n) Magnification of boxed areas in (i), with yellow arrows indicating laticifers and red arrowheads highlighting idioblasts. Bars: 0.5 mm.

Laticifers were identified in the hypocotyls of all samples, including embryos in immature seeds (Figs S6, S7). Most epidermal cells, cortical cells, and laticifers in embryos of immature seeds were filled with globular structures, likely lipid droplets (LDs, oil bodies) encased in a lipid monolayer membrane (Fig. S8). In one embryo of an immature seed, most cells, including laticifers, contained embryonic vacuoles (EVs) surrounded by a unit membrane (lipid bilayer) with an interior with a low electron density (Fig. S8a,e). Another embryo displayed what seemed to be protein storage vacuoles (PSVs) with an interior with a high electron density in epidermal and cortical cells, but no vacuoles were observed in laticifers, similar to the embryos of 0 HAG seeds (Figs 4, S8f,j).

In embryos of germinating *C. roseus* seeds, notable differences were observed between cells located near the cotyledon (Figs 4, S10) and those near the radicle (Figs S9, S11). Changes in intracellular structure typically occurred first in cells near the radicle and then in cells near the cotyledon. This analysis focused primarily on changes observed in the cells of the hypocotyl near the cotyledon.

In embryos of 0 HAG seeds, including laticifers, cells were filled with globular structures with a monolayered membrane, likely LDs (Figs 4a–c, S10a,c). Similarly, at 12 HAG, 24 HAG, and 36 HAG, many LDs were present in all cells. However, the electron density and size of LDs in laticifers differed significantly from those in epidermal and cortical cells, indicating potential differences in contents (Figs 4, S10).

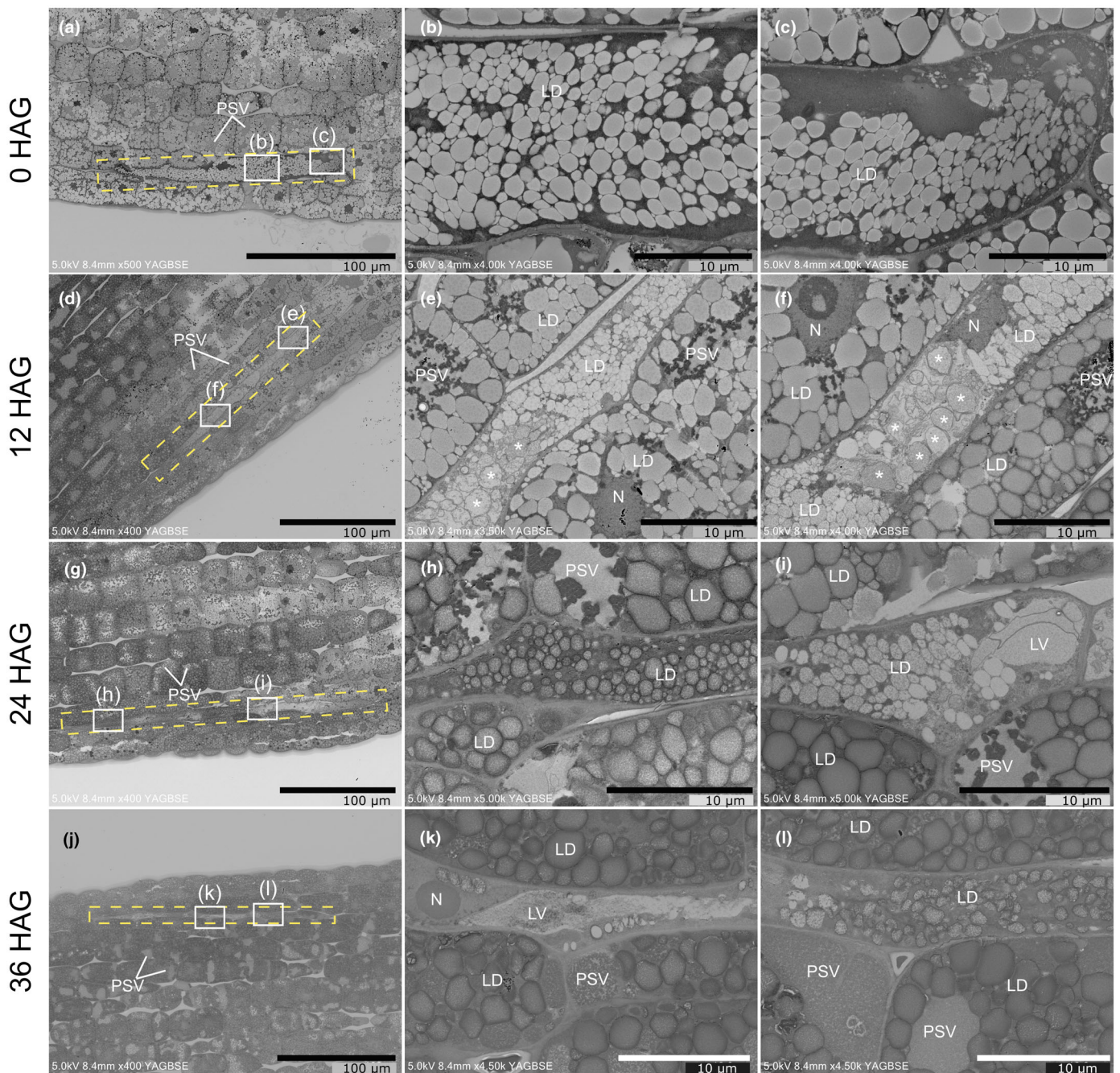


**Fig. 4** Electron micrographs of laticifers in germinating seeds of *Catharanthus roseus*. (a, d, g, j) Images of laticifers in the hypocotyl near the cotyledon of embryos at (a) 0 h after germination (HAG), (d) 12 HAG, (g) 24 HAG, and (j) 36 HAG. Elongated laticifers are highlighted within dashed yellow lines. Bars: 100 µm. (b, c, e, f, h, i, k, l) Magnifications of boxed areas in (a, d, g, or j). Bars: 10 µm. LD, lipid droplet; LV, lytic vacuole; N, nucleus; PSV, protein storage vacuole; \* in (e, f), LV-like unknown organelle.

In laticifers of 0 HAG embryos, no vacuoles were present, unlike the PSVs observed in epidermal and cortical cells (Figs 4a–c, S10a,c). Lytic vacuole (LV)-like structures with unit membranes and interiors with a low electron density emerged in laticifers of 12 HAG embryos, developing further in 24 HAG and 36 HAG embryos (Fig. 4b,l). By contrast, PSVs were observed in epidermal and cortical cells, with no LV identified in these cells on the cotyledon side throughout germination

(Fig. S10). These observations suggest that the laticifers show a significantly different cell differentiation process, compared with the surrounding cells, especially regarding the vacuole: epidermal and cortical cells store proteins, whereas laticifers store alkaloids.

Multinuclear laticifers were identified in 12–36 HAG embryos (Figs S12, S13), consistent with previous reports of nonarticulated-unbranched laticifers (Esau, 1965; Wilson & Mahlberg, 1978; Mahlberg, 1993; Hagel *et al.*, 2008).

MIA accumulation increased immediately after germination

Having found that laticifers are morphologically differentiated before seed germination and that their intracellular structure changes significantly with germination, the next step is to understand the initiation of MIA metabolism during seed germination and its correlation with cellular structural differentiation. For this purpose, time-series liquid chromatography–tandem mass spectrometry (LC–MS/MS) analysis of embryos and endosperms of mature seeds after imbibition was conducted. To determine how nutrients in seeds are allocated to MIAs during germination, the seeds were germinated without external nutrient sources and MIAs were measured per 10 embryos/endosperm, without normalizing to dry weight. Seeds germinated and grew under dark conditions.

Initially, MIAs in mature tissues were quantified for comparison with embryo composition. In mature leaves, stems, and hypocotyls, catharanthine was highly accumulated, whereas the level of tabersonine, which is biosynthesized from dehydrosecodine as happens with catharanthine, was relatively low (Figs 1, S14). Vindoline predominantly accumulated in leaves but was undetected in other tissues, indicating leaf-specific accumulation (Fig. S14). In embryos, tabersonine was highly accumulated, catharanthine levels were relatively low, and deacetylvindoline and vindoline were very low and below quantification limits (Fig. 5a). Meanwhile, compounds such as 3,4-anhydrovinblastine (synthesized from catharanthine and vindoline), along with vinblastine and vincristine were accumulated in embryos before imbibition as well as germination (Figs 1, 5a).

A detailed analysis revealed that most MIAs increased dramatically at 12 HAG (Fig. 5b). The level of catharanthine was low, almost one-hundredth of tabersonine, until 36 HAG. Similarly, serpentine levels were about one-tenth of its precursor, ajmalicine, until 36 HAG. The levels of 3,4-anhydrovinblastine, vinblastine, and vincristine gradually increased after germination. Tryptamine, strictosidine, tabersonine, catharanthine, ajmalicine, serpentine, and bis-indole alkaloids were detected in embryos before germination (0 HAI–0 HAG), although below the limit of quantification.

Iridoid compounds such as loganic acid, loganin, and secologanin in embryos and endosperms were also quantified (Fig. S15). Loganic acid levels were high before germination and decreased after germination, while loganin levels were low before germination and increased in both embryos and endosperms after germination (Fig. S15). Secologanin was detected but below the quantification limit.

Considering previous findings that vindoline biosynthesis is stimulated by red light (Liu *et al.*, 2019), MIAs in embryos from seeds germinated under light conditions were also quantified (Fig. S16). The amount of vindoline slightly increased under light conditions, but not substantially, compared with mature leaves. This suggests that MIA composition in embryos differs from that in mature tissues.

Some MIAs, including tryptamine, strictosidine, tabersonine, catharanthine, and ajmalicine, accumulated in the endosperm before imbibition (Fig. S17). After germination, the levels of these compounds increased while those of vinblastine and

vincristine decreased (Fig. S17). Deacetylvindoline, vindoline, and serpentine were also detected in endosperms but below the quantification limit.

### The expression of MIA biosynthetic enzyme genes and MIA content are well correlated

To further analyze the initiation of MIA biosynthesis by examining the timing of activation of MIA biosynthesis, time-series RNA-seq analysis of whole embryos after imbibition was conducted (Methods S6). The results revealed that the expression of most MIA biosynthetic enzyme genes increased at 12 HAG, aligning with the spike in MIA accumulation (Figs 5, S18). The expressions of the genes *T16H*, *T16H2*, *DAT*, and *SS* were too low for quantification; indeed, *T16H2* and *DAT* expression are inhibited in darkness (Liu *et al.*, 2019).

In hierarchical clustering analysis and heatmaps of *Z*-scored gene expression, MIA-related genes were divided into five clusters (Fig. 6). Many MIA biosynthetic enzyme genes were in the first and second cluster, showing increased expression during 12–24 HAG. Biosynthetic enzyme genes for the iridoid pathway expressed in IPAP cells and genes for the late pathway of vinblastine/vincristine biosynthesis were in the third cluster, with increased expression at 36 HAG (Figs 6, S18, S19). Iridoid biosynthetic enzyme genes such as *7DLGT* and *7DLH* showed increased expression at 36 HAG, whereas *LAMT* and *SLS2* expression increased at 12 HAG (Figs 6, S19).

The expression levels of certain TFs known to regulate MIA biosynthesis were correlated with those of enzyme genes. *ORCA3*, a positive regulator of *STR* identified from the T-DNA insertion line of suspension cell culture (van der Fits & Memelink, 2000), was coexpressed with *MYC2*, the master regulator of jasmonate signaling and a positive regulator of *ORCA3*, with an expression pattern similar to that of *STR* (Zhang *et al.*, 2011; Figs 6, S18, S20). *BIS 1–3*, positive regulators of iridoid biosynthesis, were coexpressed with iridoid biosynthetic genes (*GES*, *G8O*, *8HGO*, *IS*, *IO*, *7DLGT*, and *7DLH*), aligning with previous research (Van Moerkercke *et al.*, 2015, 2016; Colinas *et al.*, 2021). *GATA*, a positive regulator of *T16H2*, *T3O*, *T3R*, *D4H*, and *DAT* under PIF TF control (Liu *et al.*, 2019), was not coexpressed with any other gene analyzed in this study, and the known iridoid transporters NPF2.4 and NPF2.6 were not coexpressed with iridoid biosynthetic genes. These findings suggest that transcriptional regulation is involved in MIA biosynthesis during seed germination, but that still unknown regulators of MIA biosynthesis must exist.

### Alkaloid staining and imaging mass spectrometry analysis revealed the cellular localization of MIAs and iridoids

The localization of alkaloids in embryos was investigated using Dragendorff's reagent staining, which reacts with alkaloids to create brownish precipitates (Carqueijeiro *et al.*, 2016) (Methods S7). Laticifers in 48 HAG embryos were stained dark brown, similar to leaf section laticifers, indicating high alkaloid accumulation in laticifers in embryos (Fig. 7).



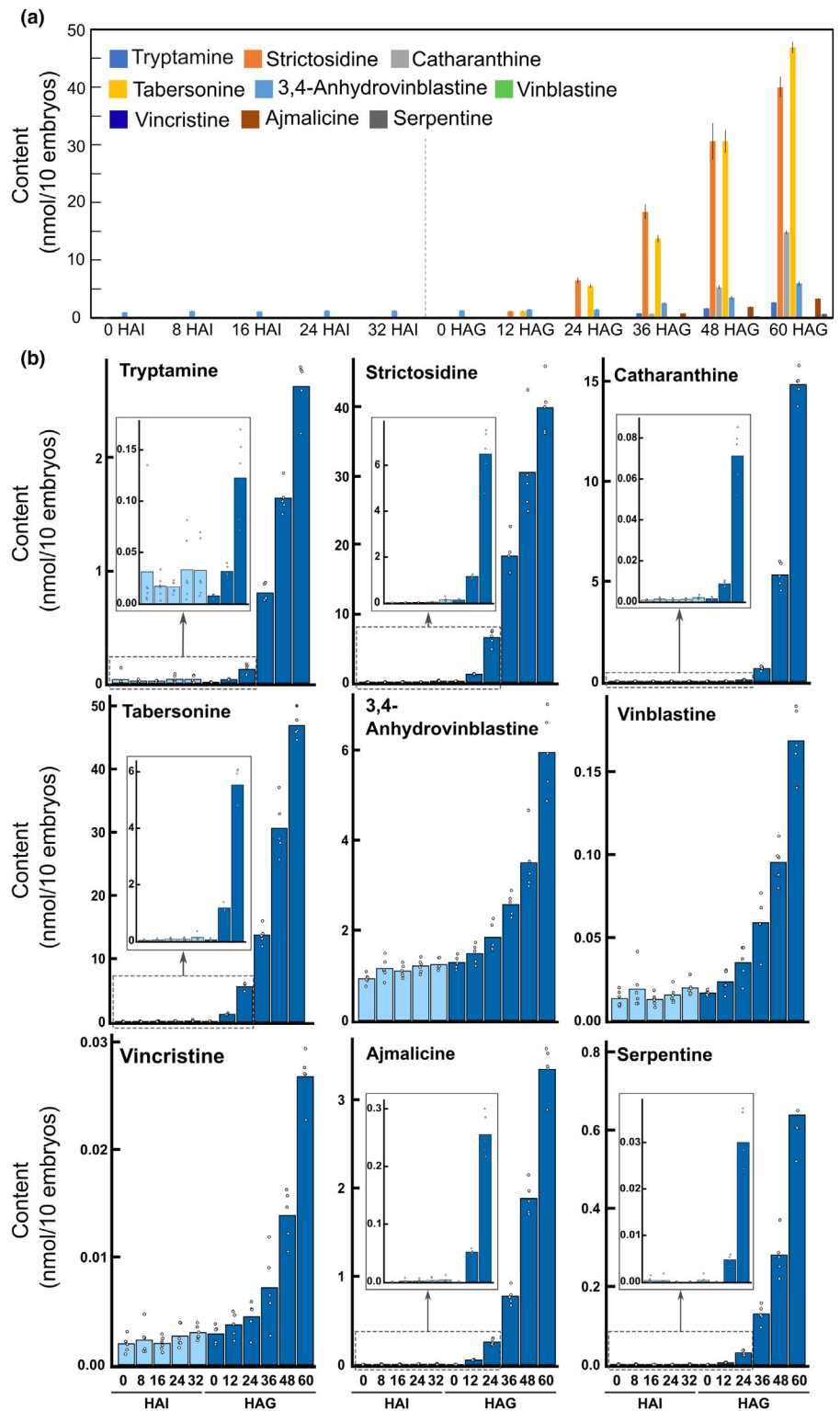


**Fig. 5** Changes in monoterpenoid indole alkaloid (MIA) content in the *Catharanthus roseus* embryo during imbibition and germination of seeds. (a) Combined plot including the levels of all quantified MIAs. Bars represent standard error (SE). (b) Individual plots for each MIA. Boxes expand the data range from 0 HAI to 24 HAG. HAI, hours after imbibition; HAG, hours after germination.  $n \geq 5$ .

Imaging mass spectrometry analysis was conducted on 24 HAG and 48 HAG germinating seeds, before and after the 36 HAG period of increased expression of iridoid biosynthetic enzyme genes and late MIA pathway enzyme genes (Fig. 6). Many compounds, including those with  $m/z$  values of 353.18, 349.15, 355.20,

337.19, 415.10, 429.11, or 427.10, were detected and annotated as MIAs or iridoids (Figs 8, S21). However, other MIAs or iridoids could not be detected, possibly due to low abundance or ionization difficulty. LC-MS/MS analysis of embryo extracts identified other compounds with these  $m/z$  values, but they could not be

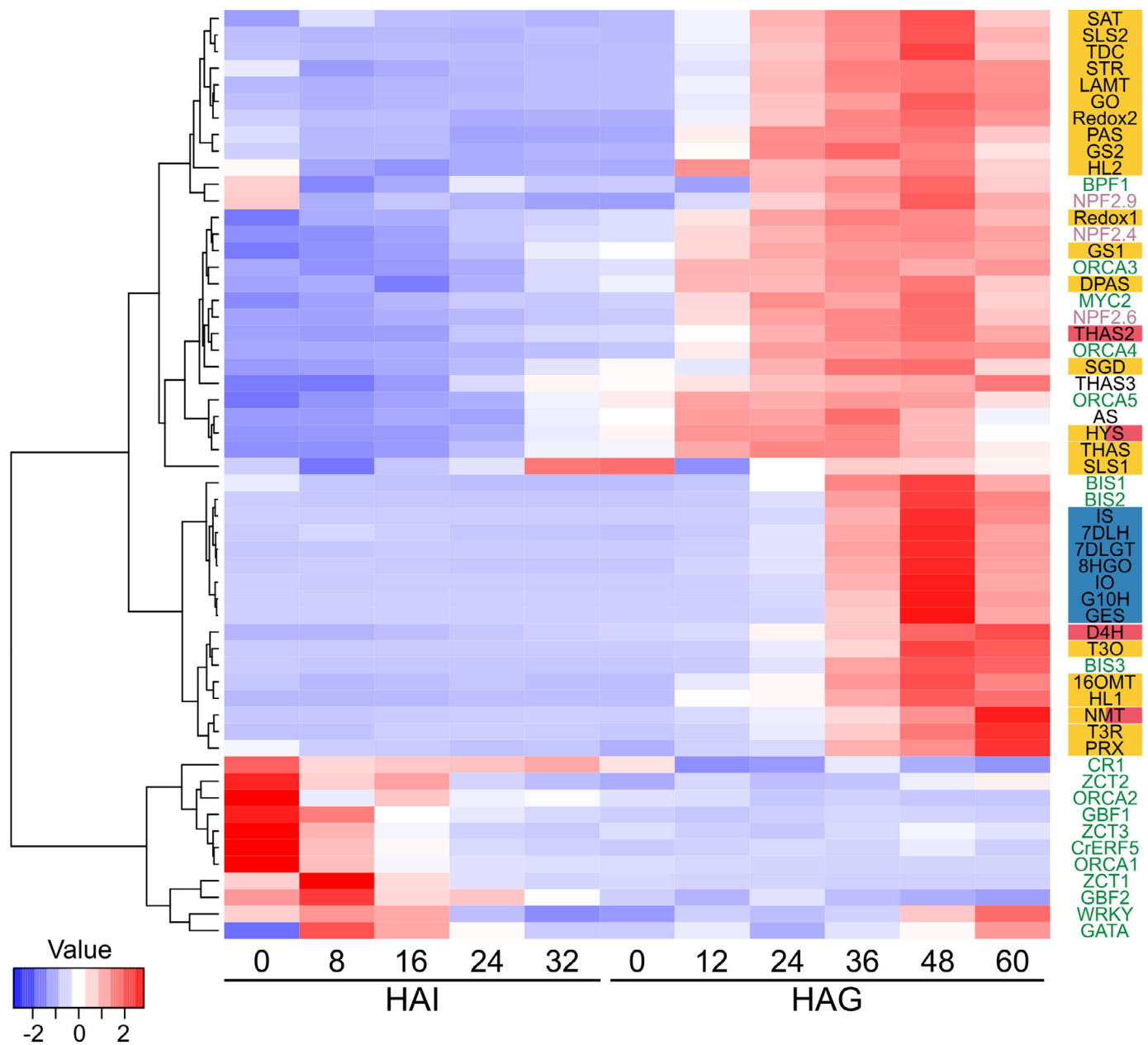


**Fig. 6** Heatmap of known monoterpene indole alkaloid (MIA) enzyme genes, Transcription factors (TFs), and transporters of *Catharanthus roseus* from RNA-seq analysis. MIA biosynthetic enzyme genes expressed in internal phloem-associated parenchyma (IPAP) cells, epidermis, and idioblasts/laticifers are surrounded in blue, yellow, and red boxes, respectively. Gene names highlighted in green represent TFs, while those in pink denote transporters. The color of each cell represents the Z-scored gene expression. Localizations of transcripts of MIA biosynthetic genes are based on single-cell transcriptome analysis of leaves (Sun *et al.*, 2022). Enzyme gene abbreviations are provided in Fig. 1. HAG, hours after germination; HAI, hours after imbibition.

definitively identified via IMS (Methods S8). Nevertheless, based on the LC-MS/MS results, it was concluded that the most abundant compounds detected with  $m/z$  values of 337.19, 353.18, and 349.15 were tabersonine, ajmalicine/tetrahydroalstonine, and serpentine, respectively (Table S2). Ajmalicine and tetrahydroalstonine could not be distinguished due to their nearly equal abundance. MIAs mainly accumulated in hypocotyls and roots,

not in cotyledons, at 24 HAG and 48 HAG (Fig. 8). Compounds at  $m/z=415.10$ , 429.11, and 427.10 were annotated as loganic acid, loganin, and secologanin, respectively, with loganic acid detected in the cotyledon at 24 HAG, and loganin and secologanin primarily in hypocotyls and roots. These results strongly suggest that alkaloids and iridoids are biosynthesized and/or accumulate in a cell type- and tissue-specific manner.

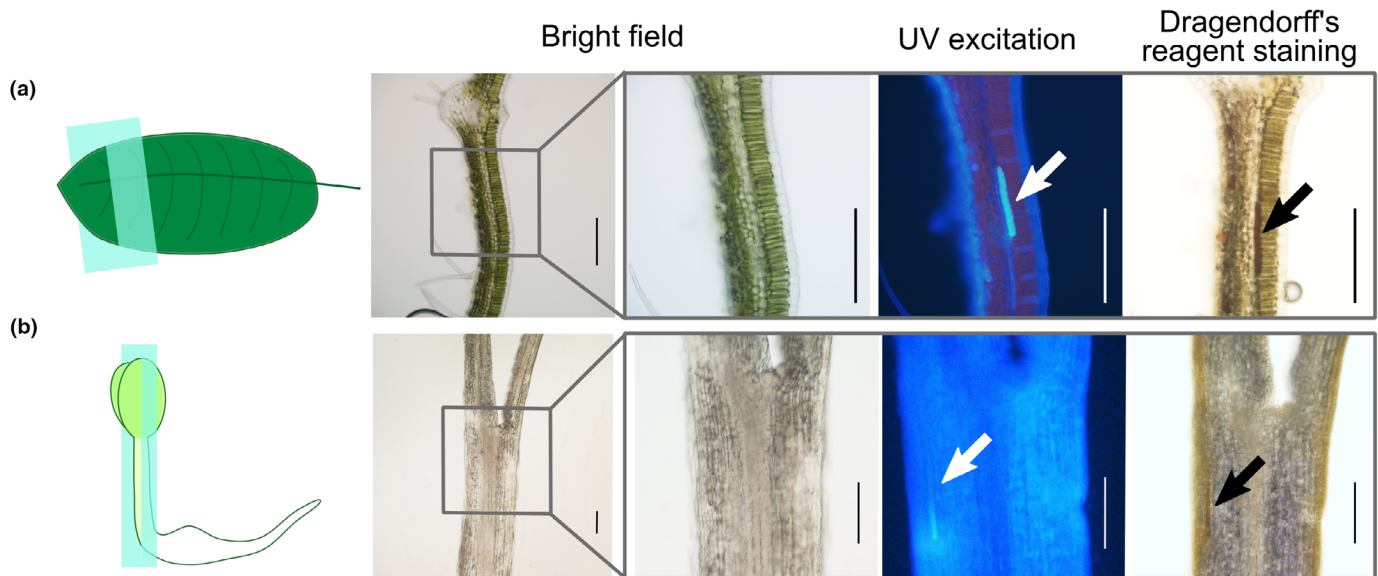


**Fig. 7** Alkaloid staining of leaf sections and 48 h after germination (HAG) embryos of *Catharanthus roseus*. Microscopic images before and after alkaloid staining with Dragendorff's reagent of sections from (a) a leaf and (b) a 48 HAG embryo. The arrows indicate laticifers. Bars: 200  $\mu\text{m}$ .

## Discussion

### Morphological differentiation of idioblasts and laticifers during embryo development in *C. roseus*

We performed detailed microscopic observation of embryos dissected from *C. roseus* seeds, both before and after maturation. The results showed that laticifers had already morphologically differentiated in developing embryos. These cells accumulated specific fluorescent compounds (Fig. 3e,g,h). This finding was unexpected, as nonarticulated-unbranched laticifers, including those in *C. roseus*, were previously thought to differentiate postembryonically in developing shoots (Esau, 1965; Hagel *et al.*, 2008). Unlike laticifers, fluorescent idioblasts were not observed at this stage. A previous study indicated that idioblasts differentiate later than laticifers in developing leaves (Uzaki *et al.*, 2022), suggesting that idioblast differentiation might not occur before seed maturation. After seed maturation and germination, fluorescent compounds accumulated in laticifers after 24 HAG. The fluorescent compound in laticifers of embryos at these stages was not solely serpentine. Despite the detection of small amounts of serpentine in embryos, the expression of serpentine synthase was almost undetectable, indicating that serpentine is unlikely the primary fluorescent substance in laticifer cells in embryos, and that the composition of fluorescent compounds differs from that in leaves and stems (Fig. S5). These fluorescent elongated cells were stained by Nile Blue reagent and Dragendorff's reagent, suggesting that they contain lipid-soluble compounds and alkaloids, similar to laticifers observed in leaves (Figs 7, S3, S4).

Electron microscopy revealed changes in intracellular structures of laticifers during seed germination (Figs 4, S8–S11). Generally, LVs are converted from PSVs in embryos during seed germination (Zheng & Staehelin, 2011). However, our observations showed no

PSVs in laticifers, with LVs appearing instead. LVs have been described to also have other different biogenetic origins depending on the cell/tissue/organ (Cui *et al.*, 2020). This suggests that laticifers differentiate LVs without differentiating PSVs, which may contribute for MIA accumulation. In addition, the smaller size and different electron density of LDs in laticifers compared with surrounding epidermal and cortical cells indicate distinct compounds in laticifer LDs. Previous studies on plants such as *Asclepias syriaca* and *Papaver somniferum* have reported laticifer ultrastructure in immature or mature embryos but none of these specifically mentioned LV structure or distinctive LD contents in laticifers (Thureson-Klein, 1970; Wilson & Mahlberg, 1978; Inamdar *et al.*, 1988). A study on *A. thaliana* reported LDs functioning as scaffolds for enzyme proteins to synthesize antimicrobial components (Shimada *et al.*, 2014), suggesting a potential link between the unique characteristics of laticifer LDs and laticifer-specific metabolism.

Multinucleate laticifers were also observed in embryos of germinating seeds (Figs S12, S13). Previous researches have suggested that nonarticulated laticifers possess multiple nuclei (Esau, 1965; Wilson & Mahlberg, 1978). This observation aligns with established findings and adds to the understanding of laticifer development in *C. roseus*.

### Induction of MIA biosynthesis in germinating seeds in *C. roseus*

Monoterpenoid indole alkaloids were present in seeds before imbibition, with a significant increase observed at 12 HAG (Fig. 5). Given that compounds such as strictosidine and tabersonine were somewhat accumulated, while vindoline was notably low in embryos, it appears that the MIA biosynthetic pathway is only partially active, up to the synthesis of tabersonine, in

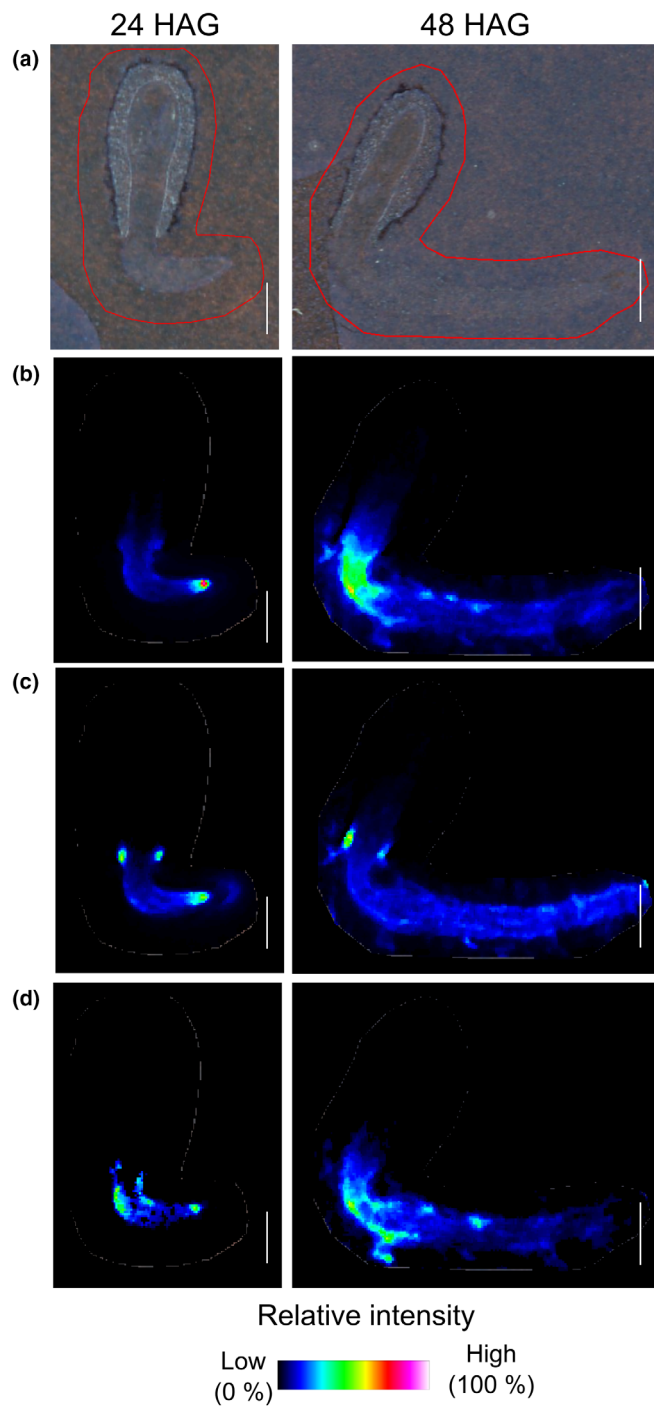


**Fig. 8** Imaging mass spectrometry (IMS) analysis of the localization of monoterpene indole alkaloids (MIAs) in the embryo of 24 h after germination (HAG) and 48 HAG seeds of *Catharanthus roseus*. (a) The images of thin sections of seeds. The areas surrounded by red line were analyzed. Distribution and concentration of (b) tetrahydroalstonine/ajmalicine ( $m/z = 353.18$ ), (c) serpentine ( $m/z = 349.15$ ), and (d) tabersonine ( $m/z = 337.19$ ) as determined by IMS analysis. Compounds are detected as  $[M + H]^+$  or  $M^+$ , and compounds for each  $m/z$  value are annotated based on nontargeted LC-MS/MS analysis (Supporting Information Table S2). Bars: 1.0 mm.

embryos of germinating seeds. Lower levels of catharanthine and serpentine compared with tabersonine or ajmalicine, particularly before 36 HAG, suggest decreased activity in their biosynthetic pathways. Enzymes such as *SS* and *DAT* were almost not expressed from 0 HAI to 60 HAG. Moreover, the expression of genes involved in the vindoline pathway (*T3O*, *T3R*, *NMT*, and *D4H*) and *HLL1* was upregulated later than genes associated with the pathway upstream of tabersonine or ajmalicine, such as *STR* and *HL2*, aligning with the observed MIA measurements (Figs 5, 6, S18).

3,4-Anhydrovinblastine, biosynthesized from catharanthine and vindoline, was present in embryos before seed imbibition and germination, although the biosynthetic enzyme genes for catharanthine and vindoline were not activated at these stages. This suggests that bis-indole alkaloids such as 3,4-anhydrovinblastine, vinblastine, and vincristine accumulate before seed maturation, independent of MIA biosynthesis initiation in germinating seed embryos. This led to the hypothesis that these compounds are transported from the mother plant or biosynthesized in embryonic tissues, before seed maturation. Furthermore, the accumulation of these bis-indole alkaloids increases later than 12 HAG, while some of the biosynthetic enzyme genes for vindoline are not expressed 0 HAI–60 HAG. We may need to also consider the existence of uncharacterized isoforms of these enzymes that are specifically expressed during embryogenesis, or the existence of another pathway for the biosynthesis of the bis-indole alkaloids via uncharacterized precursors.

Loganic acid levels were high in embryos before imbibition and decreased after germination, while loganin was almost undetectable before germination, increasing thereafter. The expression of *7DLGT* was low before germination, increasing from 36 HAG, with *LAMT* expression increasing at 12 HAG. This indicates that loganic acid is synthesized and stored during seed maturation and used after germination, with loganin, secologanin, and MIAs being biosynthesized from accumulated loganic acid (Figs 5, 6, S15, S18, S19).

Vindoline levels in embryos under light conditions were slightly elevated but still low compared with other compounds such as tabersonine (Fig. S16), suggesting an additional regulatory system for vindoline biosynthesis related to germination or growth, beyond red light regulation (Aerts & De Luca, 1992; Liu *et al.*, 2019). In two previous studies, vindoline biosynthesis was activated under light conditions in 5-d-old seedlings, indicating that further tissue or cell maturation is necessary before vindoline can be synthesized (De Luca *et al.*, 1986, 1988).

The patterns of changes in MIA accumulation correlated with the expression of MIA biosynthetic enzyme genes, indicating transcriptional regulation in the embryos of germinating seeds (Figs 5, 6, S18, S20). TFs such as *ORCA3* and *BIS 1–3* appeared to regulate some enzyme genes involved in MIA or iridoid biosynthesis. However, the distinct expression pattern of *HLL1*, which was initially upregulated and then remained stable from

12 to 24 HAG before being upregulated again after 36 HAG, and the delayed increase in expression of genes such as *16OMT1* and 2, *T3R*, *T3O*, *NMT*, *D4H*, and *PRX* compared with *STR*, were not accounted for by the expression patterns of these previously identified TFs except for *BIS 1–3* (Fig. 6). It could also be hypothesized that *BIS 1–3* might affect the expression of these genes. However, *BIS 1–3* are not coexpressed with *T16H1*, *T16H2*, *16OMT* nor *D4H* in cell culture or seedling, or the expression of *T16H1*, *T16H2*, *16OMT* nor *D4H* was not affected by overexpression of *BIS1* in hairy roots (Van Moerkercke *et al.*, 2015, 2016). Based on these facts, if *BIS 1–3* play an important role in the expression of MIA biosynthetic enzyme genes, it would be specific to embryos of germinating seeds. Alternatively, there may be other unknown regulators of these enzyme genes.

### Differences in the timing of gene expression among MIA biosynthetic enzyme genes

Time-series MIA measurements and RNA-seq analysis revealed the gradual initiation of MIA biosynthesis after 12 HAG (Figs 5, S18). Hierarchical clustering analysis and heatmapping of Z-scored gene expression identified five distinct clusters of MIA biosynthetic gene expression patterns. Notably, iridoid enzyme genes expressed in IPAP cells were in cluster 3, showing upregulation later than 24 HAG (Fig. 6). In addition, several enzyme genes for the late MIA biosynthetic pathway, such as *H11*, *16OMT1*, *16OMT2*, *T3O*, *T3R*, *NMT*, and *D4H*, were also in this cluster. *16OMT1*, *16OMT2*, *T3O*, and *T3R* convert tabersonine into vindoline or vindorosine, which are thought to accumulate in idioblasts and laticifers as well as *D4H*, and *H11* converts dehydrosecodine into catharanthine, which is also thought to accumulate mainly in idioblasts and laticifers (Yamamoto *et al.*, 2016, 2019). These findings suggest physiological reasons for the delayed synthesis and accumulation of certain MIAs, possibly linked to cellular differentiation. Future research should investigate the cellular localization of the expression of each gene and compound in embryos at various stages to validate this hypothesis.

### Metabolic differentiation of each cell and tissue

Alkaloid staining with Dragendorff's reagent revealed alkaloid accumulation in fluorescent laticifers in embryos, as well as in leaf laticifers (Fig. 7). This confirms that MIAs are highly accumulated in laticifers also in embryos. Slight staining in the epidermis suggested minor alkaloid accumulation there, aligning with previous research indicating MIA accumulation in the epidermis of young tissues (Yamamoto *et al.*, 2019). The specific MIA accumulation also supports the hypothesis that cell maturation is related to the regulation of alkaloid metabolism, as indicated by MIA measurements and transcriptome analysis. Laticifer-specific MIA accumulation was not observed from IMS analysis, which is inconsistent with Dragendorff's reagent staining analysis, due to its lower spatial resolution. The spatial resolution of IMS depends not only on the size of the laser used for ionization, but

also on various factors such as crystal size of the matrix and method of sample preparation. IMS analysis of *C. roseus* seeds requires further improvements for metabolome analysis in the single-cell level with IMS.

Fluorescence microscopy revealed that specific fluorescent compounds initially accumulated in laticifers in the roots of 24 HAG embryos, then in the hypocotyls at 36 HAG, and finally in the cotyledons at 60 HAG. Although IMS techniques could not clarify the precise cellular localization of each MIA, some MIAs were detected only in roots and hypocotyls, not in cotyledons. This suggests that MIA metabolism is initiated earlier in roots and hypocotyls than in cotyledons, consistent with the results of LC–MS/MS analysis in which vindoline, the compound that specifically accumulates in leaves, was significantly low in embryos. Loganic acid ( $m/z = 415.1001$ ) was mainly detected in cotyledons at 24 HAG but not at 48 HAG, suggesting early consumption, in line with the LC–MS/MS results (Figs S15, S21). This indicates that cotyledons at this stage might still be metabolically immature, serving primarily as accumulation sites.

In dormant seeds, metabolism is quiescent, and germination is a process of resuming metabolism. Seed germination therefore offers a valuable model for analyzing cellular metabolic differentiation. Our detailed analyses of the embryo and endosperm of germinating seeds showed that laticifers morphologically differentiate before seed maturation, MIA metabolism is induced soon after germination, and morphological differentiation precedes metabolic differentiation. Due to their toxicity, MIAs have been discussed as plant defense compounds in mature plants. The accumulation of MIAs before seed imbibition and the expression of MIA biosynthetic genes soon after germination suggest the importance of MIAs as a defense strategy also in the immature developmental phase of *C. roseus*. At the same time, the progress of cellular differentiation before the initiation of MIA biosynthesis indicates the requirement of the specific cellular environment for the MIA biosynthesis. Future research should focus on single-cell-level metabolomic and transcriptome analyses to further explore cellular metabolic differentiation.

### Acknowledgements

We extend our sincere gratitude to Dr Ikuko Hara-Nishimura (Konan University, Japan) and Dr Ryoichi Sato (RIKEN Center for Sustainable Resource Science, Japan) for their insightful discussions, to Ms. Satoko Sugawara (RIKEN Center for Sustainable Resource Science, Japan) for her assistance in IMS analysis. Special thanks are extended to Dr Robert Reid (University of Adelaide, Australia) for his valuable discussions and manuscript corrections. We also greatly appreciate the constructive comments and in-depth discussions provided by anonymous reviewers. The computational work was partially performed on the NIG supercomputer at the ROIS National Institute of Genetics. This research was funded by a Grant-in-Aid for Scientific Research of Innovative Areas from the Japanese Ministry of Education, Sports, Culture, Science, and Technology under the themes 'Perceptive plants (22120006)' and 'Plant-structure-opt (18H05493)', and by a JSPS KAKENHI grant (No. 16H04807)

to TMimura, by a JSPS KAKENHI grant (No. 22 K15136) to KY, and by a GteX Program Japan Grant No. JPMJGX23B0 to MYH. Additional support was provided by the RIKEN Junior Research Associate program and the JST SPRING, Grant No. JPMJSP2125, under the 'Interdisciplinary Frontier Next-Generation Researcher Program of the Tokai Higher Education and Research System' to MU.







## Competing interests

None declared.

## Author contributions

MU, T Mimura and MYH conceptualized the study. MU performed stereo and fluorescence microscopy, UPLC and LC-MS/MS analysis, and transcriptome analyses. T Mori carried out IMS analysis. MU and MS conducted FE-SEM observation, with MW preparing the semithin sections. MU and NT-K prepared the frozen sections for IMS. MU, KY and AM conducted fluorescence measurements of laticifers. MU and DESG performed nontargeted LC-MS/MS analysis, supported by SEOC. KT assisted with FE-SEM observation and IMS analysis. MO, CS, KI and HF contributed to manuscript preparation and data analysis. MU, T Mimura and MYH wrote the manuscript, with inputs from all authors.

## ORCID

Hidehiro Fukaki  <https://orcid.org/0000-0002-6251-7668>  
 Delia Ayled Serna Guerrero  <https://orcid.org/0000-0002-4846-1856>  
 Masami Yokota Hirai  <https://orcid.org/0000-0003-0802-6208>  
 Kimitsune Ishizaki  <https://orcid.org/0000-0003-0504-8196>  
 Tetsuro Mimura  <https://orcid.org/0000-0002-8022-3823>  
 Tetsuya Mori  <https://orcid.org/0000-0001-5347-8890>  
 Akio Murakami  <https://orcid.org/0000-0002-4662-8368>  
 Sarah E. O'Connor  <https://orcid.org/0000-0003-0356-6213>  
 Kiminori Toyooka  <https://orcid.org/0000-0002-6414-5191>  
 Mai Uzaki  <https://orcid.org/0000-0002-6181-6789>  
 Kotaro Yamamoto  <https://orcid.org/0000-0003-3817-333X>

## Data availability

The time-series RNA-seq data from this study are available in the NCBI BioProject under accession no: PRJNA910967.

## References

- Aerts RJ, De Luca V. 1992. Phytochrome is involved in the light-regulation of vindoline biosynthesis in *Catharanthus*. *Plant Physiology* 100: 1029–1032.
- Carqueijeiro I, Guimaraes AL, Bettencourt S, Martinez-Cortes T, Guedes JG, Gardner R, Lopes T, Andrade C, Bispo C, Martins NP *et al.* 2016. Isolation of cells specialized in anticancer alkaloid metabolism by fluorescence-activated cell sorting. *Plant Physiology* 171: 2371–2378.
- Castelblanque L, Balaguer B, Marti C, Rodriguez JJ, Orozco M, Vera P. 2016. Novel insights into the organization of laticifer cells: a cell comprising a unified whole system. *Plant Physiology* 172: 1032–1044.
- Colinas M, Pollier J, Vaneechoutte D, Malat DG, Schweizer F, De Milde L, De Clercq R, Guedes JG, Martinez-Cortes T, Molina-Hidalgo FJ *et al.* 2021. Subfunctionalization of paralog transcription factors contributes to regulation of alkaloid pathway branch choice in *Catharanthus roseus*. *Frontiers of Plant Science* 12: 687406.
- Cui Y, Zhao Q, Hu S, Jiang L. 2020. Vacuole biogenesis in plants: how many vacuoles, how many models? *Trends in Plant Science* 25: 538–548.
- Datta A, Srivastava PS. 1997. Variation in vinblastine production by *Catharanthus roseus* during *in vivo* and *in vitro* differentiation. *Phytochemistry* 46: 135–137.
- Dawson C. 2022. *GGPRISM: a 'GGPLOT2' extension inspired by 'GraphPad Prism'*. R package v.1.0.4. [WWW document] URL <https://cran.r-project.org/package=ggprism>
- De Luca V, Balsevich J, Tyler RT, Eilert U, Panchuk BD, Kurz WGW. 1986. Biosynthesis of indole alkaloids: developmental regulation of the biosynthetic pathway from tabersonine to vindoline in *Catharanthus roseus*. *Journal of Plant Physiology* 125: 147–156.
- De Luca V, Fernandez JA, Campbell D, Kurz WG. 1988. Developmental regulation of enzymes of indole alkaloid biosynthesis in *Catharanthus roseus*. *Plant Physiology* 86: 447–450.
- Dugé De Bernonville T, Carqueijeiro I, Lanoue A, Lafontaine F, Sánchez Bel P, Liesecke F, Musset K, Oudin A, Glévarac G, Pichon O *et al.* 2017. Folivory elicits a strong defense reaction in *Catharanthus roseus*: metabolomic and transcriptomic analyses reveal distinct local and systemic responses. *Scientific Reports* 7: 40453.
- Esau K. 1965. *Plant anatomy*. New York, NY, USA; London, UK; Sydney, NSW, Australia: John Wiley & Sons, Inc.
- Foster AS. 1955. Plant idioblasts: remarkable examples of cell specialization. *Plant Science Bulletin* 1: 184–192.
- Fujiwara T, Hirai MY, Chino M, Komeda Y, Naito S. 1992. Effects of sulfur nutrition on expression of the soybean seed storage protein genes in transgenic petunia. *Plant Physiology* 99: 263–268.
- Guedes JG, Ribeiro R, Carqueijeiro I, Guimaraes AL, Bispo C, Archer J, Azevedo H, Fonseca NA, Sottomayor M. 2024. The leaf idioblastome of the medicinal plant *Catharanthus roseus* is associated with stress resistance and alkaloid metabolism. *Journal of Experimental Botany* 75: 274–299.
- Hagel JM, Yeung EC, Facchini PJ. 2008. Got milk? The secret life of laticifers. *Trends in Plant Science* 13: 631–639.
- Hara T, Kobayashi E, Ohtsubo K, Kumada S, Kanazawa M, Abe T, Itoh RD, Fujiwara MT. 2015. Organ-level analysis of idioblast patterning in *Egeria densa* planch. *PLOS ONE* 10: e0118965.
- Harrell FE Jr, Dupont C. 2019. *Hmisc: harrell miscellaneous*. R package v.4.2-0. [WWW document] URL <https://CRAN.R-project.org/package=Hmisc>
- Inamdar JA, Murugan V, Subramanian RB. 1988. Ultrastructure of non-articulated laticifers in *Allamanda-Violacea*. *Annals of Botany* 62: 583–588.
- Kanazawa T, Morinaka H, Ebine K, Shimada TL, Ishida S, Minamino N, Yamaguchi K, Shigenobu S, Kohchi T, Nakano A *et al.* 2020. The liverwort oil body is formed by redirection of the secretory pathway. *Nature Communications* 11: 6152.
- Koroleva OA, Davies A, Deeken R, Thorpe MR, Tomos AD, Hedrich R. 2000. Identification of a new glucosinolate-rich cell type in *Arabidopsis* flower stalk. *Plant Physiology* 124: 599–608.
- Kulagina N, Meteignier LV, Papon N, O'Connor SE, Courdavault V. 2022. More than a *Catharanthus* plant: a multicellular and pluri-organelle alkaloid-producing factory. *Current Opinion in Plant Biology* 67: 102200.
- Li C, Wood JC, Vu AH, Hamilton JP, Rodriguez Lopez CE, Payne RME, Serna Guerrero DA, Gase K, Yamamoto K, Vaillancourt B *et al.* 2023. Single-cell multi-omics in the medicinal plant *Catharanthus roseus*. *Nature Chemical Biology* 19: 1031–1041.
- Liu Y, Patra B, Pattanaik S, Wang Y, Yuan L. 2019. GATA and phytochrome interacting factor transcription factors regulate light-induced vindoline biosynthesis in *Catharanthus roseus*. *Plant Physiology* 180: 1336–1350.

- Mahlberg PG. 1961. Embryogeny and histogenesis in *Nerium oleander*. II. Origin and development of the nonarticulated laticifer. *American Journal of Botany* 48: 10.
- Mahlberg PG. 1993. Laticifers—an historical-perspective. *Botanical Review* 59: 1–23.
- Miettinen K, Dong L, Navrot N, Schneider T, Burlat V, Pollier J, Woittiez L, van der Krol S, Lugin R, Ilc T *et al.* 2014. The seco-iridoid pathway from *Catharanthus roseus*. *Nature Communications* 5: 3606.
- Nakabayashi R, Hashimoto K, Toyooka K, Saito K. 2019. Keeping the shape of plant tissue for visualizing metabolite features in segmentation and correlation analysis of imaging mass spectrometry in *Asparagus officinalis*. *Metabolomics* 15: 24.
- Olsson ME, Olofsson LM, Lindahl AL, Lundgren A, Brodelius M, Brodelius PE. 2009. Localization of enzymes of artemisinin biosynthesis to the apical cells of glandular secretory trichomes of *Artemisia annua* L. *Phytochemistry* 70: 1123–1128.
- Onoyovwe A, Hagel JM, Chen X, Khan MF, Schriemer DC, Facchini PJ. 2013. Morphine biosynthesis in opium poppy involves two cell types: sieve elements and laticifers. *Plant Cell* 25: 4110–4122.
- R Core Team. 2020. *R: a language and environment for statistical computing*. Vienna, Austria: R Foundation for Statistical Computing. [WWW document] URL <https://www.R-project.org/>
- Rush MD, Kutchan TM, Coscia CJ. 1985. Correlation of the appearance of morphinan alkaloids and laticifer cells in germinating *Papaver bracteatum* seedlings. *Plant Cell Reports* 4: 237–240.
- Shimada TL, Takano Y, Shimada T, Fujiwara M, Fukao Y, Mori M, Okazaki Y, Saito K, Sasaki R, Aoki K *et al.* 2014. Leaf oil body functions as a subcellular factory for the production of a phytoalexin in Arabidopsis. *Plant Physiology* 164: 105–118.
- Shirakawa M, Ueda H, Nagano AJ, Shimada T, Kohchi T, Hara-Nishimura I. 2014. FAMA is an essential component for the differentiation of two distinct cell types, myrosin cells and guard cells in Arabidopsis. *Plant Cell* 26: 4039–4052.
- Stavrinides A, Evangelos FE, Caputi L, Kellner F, Courdavault V, O'Connor SE. 2015. Unlocking the diversity of alkaloids in *Catharanthus roseus* nuclear localization suggests metabolic channeling in secondary metabolism. *Chemistry & Biology* 22: 336–341.
- St-Pierre B, Vazquez-Flota FA, De Luca V. 1999. Multicellular compartmentation of *Catharanthus roseus* alkaloid biosynthesis predicts intercellular translocation of a pathway intermediate. *Plant Cell* 11: 887–900.
- Suire C. 2000. A comparative, transmission-electron microscopic study on the formation of oil-bodies in liverworts. *Journal of the Hattori Botanical Laboratory* 89: 209–232.
- Sun S, Shen X, Li Y, Li Y, Wang S, Li R, Zhang H, Shen G, Guo B, Wei J *et al.* 2022. Single-cell RNA sequencing provides a high-resolution roadmap for understanding the multicellular compartmentation of specialized metabolism. *Nature Plants* 9: 179–190.
- Thureson-Klein A. 1970. Observations on the development and fine structure of the articulated laticifers of *Papaver somniferum*. *Annals of Botany* 34: 9–759.
- Uzaki M, Yamamoto K, Murakami A, Fuji Y, Ohnishi M, Ishizaki K, Fukaki H, Hirai MY, Mimura T. 2022. Differential regulation of fluorescent alkaloid metabolism between idioblast and laticifer cells during leaf development in *Catharanthus roseus* seedlings. *Journal of Plant Research* 135: 473–483.
- Van der Fits L, Memelink J. 2000. ORCA3, a jasmonate-responsive transcriptional regulator of plant primary and secondary metabolism. *Science* 289: 295–297.
- Van Der Heijden R, Jacobs DI, Snoeijer W, Hallard D, Verpoorte R. 2004. The *Catharanthus* alkaloids: pharmacognosy and biotechnology. *Current Medical Chemistry* 11: 607–628.
- Van Moerkercke A, Steensma P, Gariboldi I, Espoz J, Purnama PC, Schweizer F, Miettinen K, Vanden Bossche R, De Clercq R, Memelink J *et al.* 2016. The basic helix-loop-helix transcription factor BIS2 is essential for monoterpenoid indole alkaloid production in the medicinal plant *Catharanthus roseus*. *The Plant Journal* 88: 3–12.
- Van Moerkercke A, Steensma P, Schweizer F, Pollier J, Gariboldi I, Payne R, Vanden Bossche R, Miettinen K, Espoz J, Purnama PC *et al.* 2015. The bHLH transcription factor BIS1 controls the iridoid branch of the monoterpenoid indole alkaloid pathway in *Catharanthus roseus*. *Proceedings of the National Academy of Sciences, USA* 112: 8130–8135.
- Weng JK, Lynch JH, Matos JO, Dudareva N. 2021. Adaptive mechanisms of plant specialized metabolism connecting chemistry to function. *Nature Chemical Biology* 17: 1037–1045.
- Wickham H. 2016. *GGPLOT2: elegant graphics for data analysis*. New York, NY, USA: Springer-Verlag.
- Wickham H. 2023. *STRINGR: simple, consistent wrappers for common string operations*. R package v.1.5.1. [WWW document] URL <https://github.com/tidyverse/stringr>, <https://stringr.tidyverse.org>
- Wickham H, Averick M, Bryan J, Chang W, McGowan L, François R, Grolemond G, Hayes A, Henry L, Hester J *et al.* 2019. Welcome to the Tidyverse. *Journal of Open Source Software* 4: 1686.
- Wickham H, François R, Henry L, Müller K, Vaughan D. 2023. *DPLYR: a grammar of data manipulation*. R package v.1.4. [WWW document] URL <https://github.com/tidyverse/dplyr>
- Wilson KJ, Mahlberg PG. 1978. Ultrastructure of non-articulated laticifers in mature embryos and seedlings of *Asclepias-Syriaca* L (Asclepiadaceae). *American Journal of Botany* 65: 98–109.
- Yamamoto K, Takahashi K, Caputi L, Mizuno H, Rodriguez-Lopez CE, Iwasaki T, Ishizaki K, Fukaki H, Ohnishi M, Yamazaki M *et al.* 2019. The complexity of intercellular localisation of alkaloids revealed by single-cell metabolomics. *New Phytologist* 224: 848–859.
- Yamamoto K, Takahashi K, Mizuno H, Anegawa A, Ishizaki K, Fukaki H, Ohnishi M, Yamazaki M, Masujima T, Mimura T. 2016. Cell-specific localization of alkaloids in *Catharanthus roseus* stem tissue measured with imaging MS and single-cell MS. *Proceedings of the National Academy of Sciences, USA* 113: 3891–3896.
- Zhang H, Hedhili S, Montiel G, Zhang Y, Chatel G, Pré M, Gantet P, Memelink J. 2011. The basic helix-loop-helix transcription factor CrMYC2 controls the jasmonate-responsive expression of the ORCA genes that regulate alkaloid biosynthesis in *Catharanthus roseus*. *The Plant Journal* 67: 61–71.
- Zheng H, Staehelin LA. 2011. Protein storage vacuoles are transformed into lytic vacuoles in root meristematic cells of germinating seedlings by multiple, cell type-specific mechanisms. *Plant Physiology* 155: 2023–2035.

## Supporting Information

Additional Supporting Information may be found online in the Supporting Information section at the end of the article.

**Fig. S1** Sample preparation procedure for imaging mass spectrometry (IMS) analysis.

**Fig. S2** Changes in germination rate of *Catharanthus roseus* seeds after the start of imbibition.

**Fig. S3** Microphotographs of sections of embryo dissected from 48 h after germination (HAG) seeds.

**Fig. S4** Nile blue staining of leaves and embryos of 48 h after germination (HAG) seeds.

**Fig. S5** Comparison of fluorescence spectra of laticifers.

**Fig. S6** Microphotographs of semithin sections of embryos dissected from immature seeds.

**Fig. S7** Microphotographs of semithin sections of embryos dissected from germinating seeds.

**Fig. S8** Electron micrograph images of laticifer in embryos dissected from immature seeds.

**Fig. S9** Electron micrograph images of laticifer in the hypocotyl near the radicle.

**Fig. S10** Electron micrographs of the epidermal and cortical cells around the laticifer in the hypocotyl near the cotyledon.

**Fig. S11** Electron micrographs of epidermal and cortical cells around the laticifer in the hypocotyl near the radicle.

**Fig. S12** Electron micrographs of laticifers with two nuclei found in embryos of 12 and 24 h after germination (HAG) seeds.

**Fig. S13** Electron micrographs of multinucleated laticifers found in embryos of 36 h after germination (HAG) seeds.

**Fig. S14** Monoterpene indole alkaloid content of mature tissues.

**Fig. S15** Changes in embryo and endosperm iridoid content during seed imbibition and germination.

**Fig. S16** Monoterpene indole alkaloid content changes in embryos dissected from seeds germinated under light.

**Fig. S17** Changes in endosperm monoterpene indole alkaloid content during seed imbibition and germination.

**Fig. S18** Expression patterns of monoterpene indole alkaloid biosynthetic enzyme genes in embryos from imbibing and germinating seeds.

**Fig. S19** Expression patterns of iridoid biosynthetic enzyme and related transcription factor genes in embryos of imbibing and germinating seeds.

**Fig. S20** Expression patterns of transcription factors related to monoterpene indole alkaloid biosynthesis in embryos of imbibing and germinating seeds.

**Fig. S21** Localization of compounds annotated as loganic acid, loganin, or secologanin.

**Methods S1** Nile blue staining of embryos and leaves.

**Methods S2** Fluorescence measurement.

**Methods S3** Compound analysis using a liquid chromatography (LC) fluorescence detector.

**Methods S4** Preparation of semithin embryo sections.

**Methods S5** Observation of resin-embedded sections by field emission scanning electron microscope (FE-SEM).

**Methods S6** RNA extraction and transcriptome analysis.

**Methods S7** Alkaloid staining of section of the leaf and 48 h after germination (HAG) embryos with Dragendorff's reagent.

**Methods S8** Nontargeted metabolomic LC-tandem mass spectrometry (MS/MS) analysis.

**Table S1** Analytical condition for liquid chromatography–tandem mass spectrometry (LC–MS/MS).

**Table S2** Normalized peak intensity of compounds with  $m/z = 337.19, 349.15, 353.18, \text{ or } 355.20$  detected through nontargeted LC–MS/MS analysis.

Please note: Wiley is not responsible for the content or functionality of any Supporting Information supplied by the authors. Any queries (other than missing material) should be directed to the *New Phytologist* Central Office.